Effect of Sm doping ZnO nanorods on structural optical and electrical properties of Schottky diodes prepared by chemical bath deposition

MAM Ahmed[a,b], BS Mwankemwa[a,c], E Carleschi[d], B P Doyle[d], WE Meyer[a], JM Nel[a]

[a]*Department of physics, University of Pretoria, Private Bag X20, 0028 Hatfield, South Africa*
[b]*Department of Physics, University of Khartoum, Faculty of Education, P O Box 461, Omdurman, Sudan*
[c]*Department of Physics, School of Physical Sciences, University of Dodoma, P O Box 338, Dodoma, Tanzania*
[d]*Department of Physics, University of Johannesburg, P O Box 524, Auckland Park, South Africa*

Abstract

In this study, pure and Sm doped ZnO nanorods from 0.0 to 5.5 at.% were synthesized using the chemical bath deposition method at 90° C. The effect of Sm doping of ZnO nanorods on their structural, morphology and optical properties were investigated. X-ray diffraction patterns revealed that Sm had been successfully incorporated into the ZnO lattice and no other impurities or Sm oxide phases were detected. Field emission scanning electron microscopy images showed that the growth rate of the nanorods was suppressed by Sm doping. Room temperature Raman scattering spectroscopy revealed that the relative intensity of $E_2(high)$ mode decreased and shifted slightly towards a lower wavenumber in Sm doped ZnO when compared to the undoped ZnO nanorods. The photoluminescence spectrum of as-synthesized Sm-doped samples measured at room temperature shows that the UV emission is slightly red shifted and the green-yellow emission of the visible emission is enhanced, when compared to undoped samples. Photoluminescence studies also revealed the good crystal quality of the as-synthesized samples as all sample shows strong ultraviolet and weak deep-level emission peaks. The as-synthesized samples were also characterized using X-ray photoelectron spectroscopy that revealed the presence of Zn and O in all samples and a small amount of Sm in 5.5 at.% Sm doped ZnO was detected. Furthermore, the current-voltage characteristics of a fabricated Schottky diodes showed a good rectifying behavior when ZnO doped with Sm at 1.5 at.%. The obtained Schottky barrier height for pure and Sm doped ZnO nanorods were 0.55 eV and 0.72 eV, respectively.

Keywords: ZnO, chemical bath deposition, structural properties, optical properties, electrical properties.

1. Introduction

Zinc oxide, as a semiconductor material with a direct band gap (3.20 - 3.37 eV) and large exciton binding energy (60 meV) at room temperature, has attracted much interest due to it is unique properties and potential use in a wide range of devices such as photodiodes [1, 2, 3, 4], single electron transistors [5] and sensing applications [6]. It is believed that zinc oxide is one of the environmentally friendly candidates that can be used in nanodevices. ZnO is also used as host material for luminescence centres. One of the most effective ways to alter the electrical and optical properties of ZnO is doping with cations [7, 8, 9]. Previous reports have shown that dopants such as Ga and Al can improve the optical and electrical properties of the ZnO thin films [10, 11, 12]. ZnO doped metal nanostructures such as Mn [13] and Al [14] are very promising for the applications in nonlinear optics. Rare-earth element (RE) such as Eu [15], Tb [16], Er, La, Yb [17] and Sm [18] have been recently used as dopant for ZnO. These RE doped semiconductors modify effectively the emission in the visible part making them good candidates for phosphors and multicolored LEDs [19]. These materials also show a strong florescence in a wide spectral range and upconversion, downconversion emission at low excitation power. The presence of the RE ions are accomplished with energy transfer from the host semiconductors. Zeng *et al.* observed energy transfer in ZnO doped Eu^{+3} nanosheets [20]. RE doping ions act as effective luminescence centers in the green and red region. Sm doped ZnO has also showed a good optical properties,

Email address: mustafa.sonbl@gmail.com (MAM Ahmed)

He and co-workers found that Sm doped ZnO thin film has enhanced the green emission [21, 22]. Moreover, Sm doping ZnO is gaining attention due to the number of advantages such that it improves optical, electrical and magnetic properties as well as surface roughness, scintillation, luminescence and oxygen gain compared to commonly and widely used Al which only reported to improve electrical properties and decreasing the optical transmittance window of ZnO [23].

Various techniques have been used to synthesize ZnO nanoparticles, for example chemical vapor deposition [24], pulse laser deposition [25], molecular beam epitaxy [26], sol-gel [27] and chemical bath deposition (CBD) [28, 29, 30]. In this study we report on the synthesis, structural and optical properties of pure and Sm doped ZnO nanorods using CBD. The CBD method was used because it is a simple experimental setup, low temperature and inexpensive technique. ZnO has been grown on different substrates such as Si [31], sapphire [32], GaN [33] and ITO (indium tin oxide) substrates [34]. The ITO substrate wast adopted for this study due to it is transparency in the visible region and low price compared to the Si and GaN substrates, respectively. Moreover, to our best of knowledge few reports available that compare the Raman vibration modes for undoped and Sm doped ZnO. This also motivated the use of ITO coated glass substrate because Si normally shows very high intensity peak that suppress the vibrational modes of ZnO. The purpose of this study is to investigate the effect of Sm doping on the crystallization, photoluminescence, Raman scattering, UV-vis, and electrical properties at room temperature. The electrical characterization were performed on a fabricated Schottky diodes. The study employed low temperature and shorter growth time (90 °C, 2 h) CBD method in an open beaker, which is the simplest solution based technique compared to study previously reported for Sm doped ZnO nanorods, where hydrothermal method at a temperature of 96° C for 5 h [18].

2. Material and method

2.1. Materials

All reagents used in the experiments were used as purchased without any further purification. The following starting materials were used: zinc acetate dihydrate $Zn(CH_3COO)_2.2H_2O$ (98%, Merck), zinc nitrate hexahydrate $Zn(NO_3)_2.6H_2O$ (98%, Sigma Aldrich), monoethanolamine (MEA) C_2H_7NO (98%, Merck), hexamethylenetetramine $C_6H_{12}N_{14}$ (99.5%, Sigma Aldrich) and samarium nitrate hexahydrate $Sm(NO_3)_3.6H_2O$ (99.999%, Sigma Aldrich).

2.2. Seed layer preparation

Zinc acetate (0.05 M) was dissolved in 60 ml ethanol and the solution was stirred at 300 rpm for 30 minutes, where after 1 ml of MEA was added drop-wise into the solution with a continuous stirring for 2 hours. The clear and transparent solution was aged for 24 hours, increasing the viscosity of the solution. It should be mentioned that the molar ratio of zinc acetate to MEA was kept 1:1. ITO substrates were cleaned with ethanol, deionized water, acetone and deionized water ultrasonically 5 minutes each, in this sequence and finally nitrogen gas was used to blown the substrates dry. Pre-cleaned substrate were spin-coated with 3 layers of the solutions at 4000 rpm for 40 seconds, and thereafter dried in an oven for 10 minutes at 90° C to remove any remaining residual solvents.

2.3. Growth of the nanorods

Pure ZnO nanorods were grown from ZnO seeds using CBD. Pre-coated ITO substrates with an undoped ZnO seed layer were immersed into an aqueous solution of zinc nitrate hexahydrate (0.05 M) and hexamethylenetetramine (0.05 M). All the ingredients were measured with high accuracy using Sartorius digital balance with 4 decimal places and Socorex 100 ml micro-pipette for measuring the solvents. The bath solution was placed in a hot water bath preheated to 90° C and the temperature was maintained constant throughout the deposition. Substrates were placed with their seeded side facing downward. The dopant precursor was samarium nitrate hexahydrate. Different concentrations of the dopant (0.0, 1.5, 4.0 and 5.5) at.% were used to study the effect on the structural and optical properties of wurtzite ZnO nanorods. It should be mentioned that the zinc and the dopant sources were dissolved separately, stirred for 10 minutes and finally mixed together and stirred again for another 15 minutes to make sure the homogeneous solution are obtained. This was done for all concentrations mentioned above. The deposition time for all samples was 2h.

2.4. Fabrication of Schottky contact

circular Pd contacts were deposited using vacuum resistive evaporation with a mechanical shadow mask placed on top of the nanorods for electrical measurements. The deposition rate, the vacuum pressure and the final thickness of the Pd were 0.01 nm/s, 10^{-5} torr pressure and 100 nm, respectively. Hence, Pd/ZnO/ITO Schottky diodes of pure and Sm doped ZnO nanorods have been fabricated.

2.5. Characterization

The as-synthesized products were characterized in terms of their structure and morphology with X-ray diffraction (XRD) on PANanlytical X'Pert PRO machine (λ = 1.5405 nm) and a field emission scanning electron microscopy (FE-SEM, JEOL 6000F), respectively. The Raman studies of as-synthesized samples was measured using Jobin Yvon, Horiba© TX64000 with excitation wavelength λ = 514.5 nm in the range 200 - 1800 nm. The photoluminescence spectroscopy of as-synthesized samples was used to study the optical emission in the range 360 - 800 nm using Cary Eclipse fluorescence spectrometer with excitation wavelength λ = 341 nm. Optical transmittance of as-synthesized samples was measured using a Varian Cary 100 UV-vis spectrometer. Before UV-vis transmittance, the background correction were done using a cleaned blank ITO coated glass substrate. X-ray photoelectron spectroscopy (XPS) data were acquired at room temperature with a SPECS Phoibos 150 electron energy analyser, using a monochromatized Al Kα photon source (hν = 1486.71 eV). The overall energy resolution was set to 0.5 eV for all the spectra. The binding energy was calibrated with respect to the main peak in the C 1s core level (284.6 eV), according to the procedure reported by Zheng *et al.* [35]. To counteract the effect of surface charging, samples were irradiated with a low energy electron flood gun during measurements (electron energy: 2 eV, emission current: 20 μA). Finally, electrical properties of as-synthesized samples were characterized on fabricated Schottky diodes at room temperature using HP 4140B pA meter /DC voltage source.

3. Results and discussion

3.1. Structural and morphological results

XRD patterns of ZnO nanorods and Sm-doped ZnO are shown in Fig. 1. All peaks in the XRD pattern were assigned to the wurtzite structure of ZnO and the ITO substrate. There were no diffraction peaks from samarium oxides or other impurities observed in the XRD data. The peak position of the (002) plane is slightly shifted to the lower angle (see Table 1). This indicates that Sm ions have been successfully incorporated into the ZnO lattice without any other crystalline phases. It is clear from Fig. 1 that the preferred orientation of the growth for all samples is along the reflection plane (002). The preferential (002) plane peak intensity increases slightly with increasing Sm content as compared to the undoped samples. However, the intensity of peaks along reflection planes (100) and (101) decreased with increasing the doping concentrations. The lattice parameters were calculated from XRD patterns using the following equation:

$$\frac{a^2}{d^2} = \frac{4}{3}\left[h^2 + hk + k^2\right]\frac{a^2 l^2}{c^2} \tag{1}$$

where a and c are the lattice constants, d and (hkl) represents the interplanar distance and Miller indices, respectively. The results are shown in Table 1. The obtained lattice parameters are in a good agreement with a previously reported Sm doped ZnO [36]. The decrease in lattice parameters indicates that Sm^{+3} ions replaced the Zn^{+2} in the hexagonal structure. Similar changes in the lattice parameters have been reported in Sm [36, 37] and Ce[38] doped ZnO nanoparticles. This variation in the lattice constants is due to larger ionic radii of Sm^{+3} (0.0964 nm) compared to Zn^{+2} (0.074 nm) [37]. The increase in lattice parameters at higher Sm concentration may be due to a defect induced by Sm doping. It should be mentioned that the lattice parameters are related to some factors such as concentration of impurity atoms including the difference in ionic radii, defect, and strain developed due to the temperature and pressure [39]. The average crystallites size (D) of the samples was calculated using the Scherrer equation [40]

$$D = \frac{0.9\lambda}{B\cos\theta} \tag{2}$$

where, λ is the wavelength of the X-rays, B is full width at half maximum (FWHM) of the XRD peak and θ is the Bragg angle, and the volume was calculated using $V = a^2 c \sin 120^\circ$ [36].

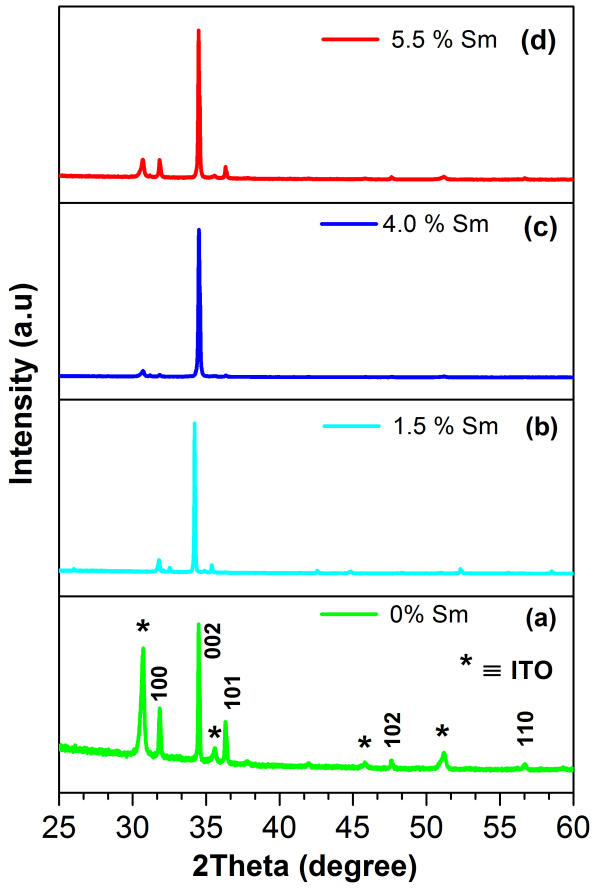

Figure 1: (Color online) XRD patterns of as synthesized samples. (a) 0 at.%Sm, (b) 1.5 at.%Sm, (c) 4.0 at.%Sm and (d) 5.5 at.%Sm.

Table 1: Lattice parameters, FWHM, particles size, volume and thickness of as-synthesized samples.

Samples	Lattice parameter (Å)		FWHM	Position (002)	Particles size (Å)	Volume	Height
at.%Sm	a	c	(002)	(degree)	(002)	(Å^3)	(nm)
0.0	3.249	5.207	0.085	34.49	24.84	47.59	1500
1.5	3.249	5.206	0.101	34.47	20.76	47.59	717
4.0	3.247	5.202	0.134	34.51	15.76	47.48	778
5.5	3.250	5.205	0.095	34.48	22.22	47.61	761

Fig. 2 shows SEM images of pure and Sm doped ZnO nanorods for all doping concentrations (0, 1.5, 4.0 and 5.5 at.%Sm). It is clear from Fig. 2 that the nanorods have the hexagonal wurtzite structure. The measured diameter and height of pure and Sm doped ZnO nanorods are in range ~ 50 - 150 nm and ~ 700 – 1500 nm, respectively. The height of the nanorods decreased with increasing the Sm content. It can be seen from Fig. 2a that the undoped nanorods grew in a very high density area compared to Fig. 2 b, c and d. This indicates that Sm affected the growth of the nanorods on the seed layer. It should be mentioned that the seed layer for all samples was undoped ZnO.

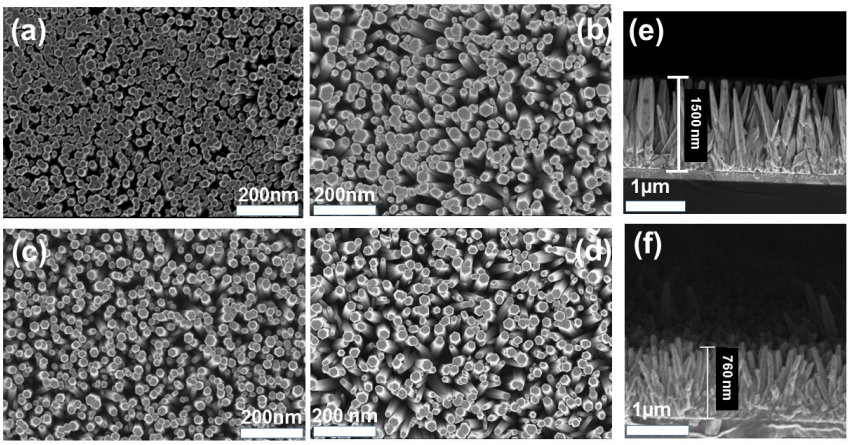

Figure 2: SEM images of ZnO: Sm nanorods. (a) 0 at.%Sm, (b) 1.5 at.%Sm, (c) 4.0 at.%Sm and (d) is 5.5 at.%Sm. The length of the nanorod for pure and 5.5 at.% Sm doped ZnO are shown in (e) 1500 nm and (f) 761 nm, respectively.

3.2. Raman

The phase purity and crystallinity of as-synthesized samples have also been investigated using Raman spectroscopy. Fig. 3 shows the Raman spectra of as-synthesized pure and Sm doped ZnO nanorods in range 200 to 1800 cm^{-1}. Only optical phonons at the Brillouin zone (Γ) are involved in the first order Raman scattering. According to the group theory calculation the following modes exist:

$$\Gamma_{Optical} = A_1 + 2B_1 + E_1 + 2E_2 \tag{3}$$

where, B_1 is silent mode, A_1, E_1 and E_2 are the first order Raman active modes according to the Raman rule selection. Both A_1 and E_1 are polar and split into transverse optical (TO) and longitudinal optical (LO) components. The E_2 mode is composed of low and high frequency phonons. The peaks in the spectra can be assigned to the lattice vibration of ZnO wurtzite structure, space group $C^4_{6v}(P6_3mc)$ [41]. The peak at 335 cm^{-1} is a multiphonon process (E_2 high - E_2 low) and E_2 high mode is at 440 cm^{-1}. The peak at 440 cm^{-1} appears to be sharp and narrow and dominates in the Raman scattering spectra, a good indication that as-synthesised samples have high crystallinity, and is supported by the XRD results. As one can see in the inset of Fig. 3, the peaks at 440 cm^{-1} are slightly shifted towards lower wavenumber when increasing the Sm doping concentration. This shift could be due to the formation of defects in the samples as the Sm content increases [18]. It should be mentioned that the FWHM increased on doping for the peak at 440 cm^{-1} E_2 (high) (see Table 2). However, for the multiphonons process, the FWHM decreased with increasing dopant. The slight changes in the FWHM at 440 cm^{-1} peaks maybe due to the Sm doping. For 0 at.% Sm ZnO nanorods a broad peak is observed around 560 cm^{-1} and it becomes more pronounce at higher Sm content, which is attributed to longitudinal optical mode with A_1 symmetry, A_1(LO). This broad peak has been seen in pure ZnO, which has a variety of defects [42]. The broad peak between 1100 and 1200 cm^{-1} is attributed to the multiphonons process (2LO) and it is a characteristic feature of II - VI semiconductors [41, 42, 43, 44]. Finally the peak at 1555 cm^{-1} originates from the ITO glass substrate.

3.3. Optical properties

3.3.1. UV-vis

The transmittance (T) spectra of pure and Sm doped ZnO nanorods at different concentrations over the wavelength range 200 - 800 nm is shown in Fig. 4 (A). As can be seen, the transmittance increases initially and then decreases with increasing the Sm content, and the maximum transmittance in the visible region being at Sm concentration of at 1.5 at.%. For example at wavelength of 570 nm, the optical transmittance increased from 62 % (undoped) to 67 % and

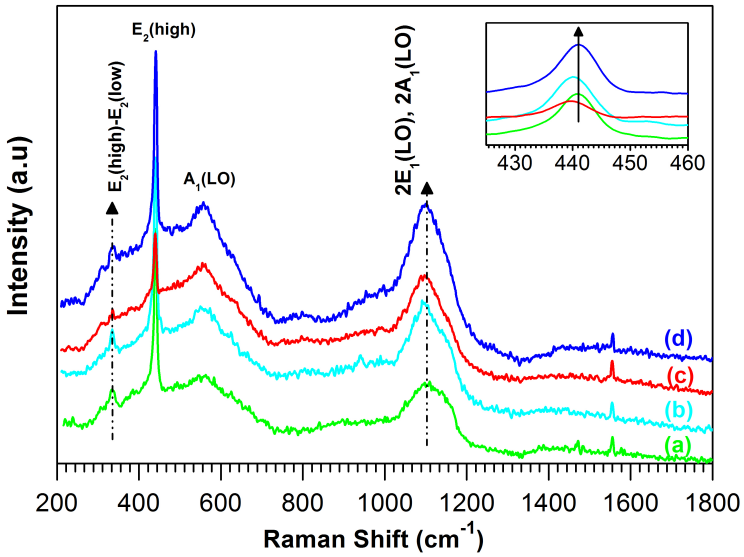

Figure 3: (Color online) Raman spectra of pure and Sm doped ZnO nanorods at different concentrations: (a) 0, (b) 1.5, (c) 4.0 and (d) 5.5 at.% Sm. The inset shows an enlargement of the peaks at 440 cm^{-1} .

Table 2: Raman shift peak position of E_2(high) mode and FWHM cm^{-1} of E_2(high) mode and the multiphonon process (E_2(high) - E_2(low)).

Concentrations	Peak Position	FWHM (cm^{-1})	
(at.%)	E_2(high)	E_2(high) - E_2(low)	E_2(high)
0.0	440.57	22.06	7.53
1.5	440.00	12.69	7.74
4.0	439.42	8.53	8.30
5.5	441.15	4.37	9.05

sharply decreased to 36 % and then increased to 46 % for 1.5, 4.0 and 5.5 at.% Sm doped, respectively. Similar trends were also reported by He *et al.* [22]. The average transmittance is in the range between ∼46 - 72 %. The increase in the transmittance with 1.5 at. % Sm content compared to the pure ZnO maybe due to shortening in the nanorods (see Table. 1). The subsequent lowering of the transmittance may due to the scattering of light by the nanorods. The broad peak between ∼ 300 - 372 nm for higher doped samples is possibly due to the defects formed in the rods.

Since the band gap of wurtzite ZnO is a direct band gap, the optical band gap can be calculated using Tauc's law [45]:

$$(\alpha h\nu)^2 = C(h\nu - E_g) \tag{4}$$

where, α is the absorption coefficient, $h\nu$ is the phonon energy, C is constant and E_g is the optical energy gap. The absorption coefficient can be calculated using equation [45]:

$$\alpha = (\frac{1}{d})\ln(\frac{1}{T}) \tag{5}$$

where d represents the thickness of the nanorods and T is transmittance. The optical band gap can be obtained by substituting Eq. 5 in Eq. 4 and plotting $(\alpha h\nu)^2$ vs. $h\nu$. The values of the optical band gap obtained when straight-line portion is extrapolated to zero as shown in Fig. 4 (B). The obtained E_g values for 0, 1.5, 4.0 and 5.5 at.%Sm are found to be 3.24, 3.28, 3.40 and 3.36 eV, respectively. The E_g values increase with increasing Sm content. The widening in the band gap compared to the undoped sample may be due the well known Moss-Burstein effect [46, 47, 10]. The decrease in the optical band gap at higher concentration may be due to the further increase of the Sm content.

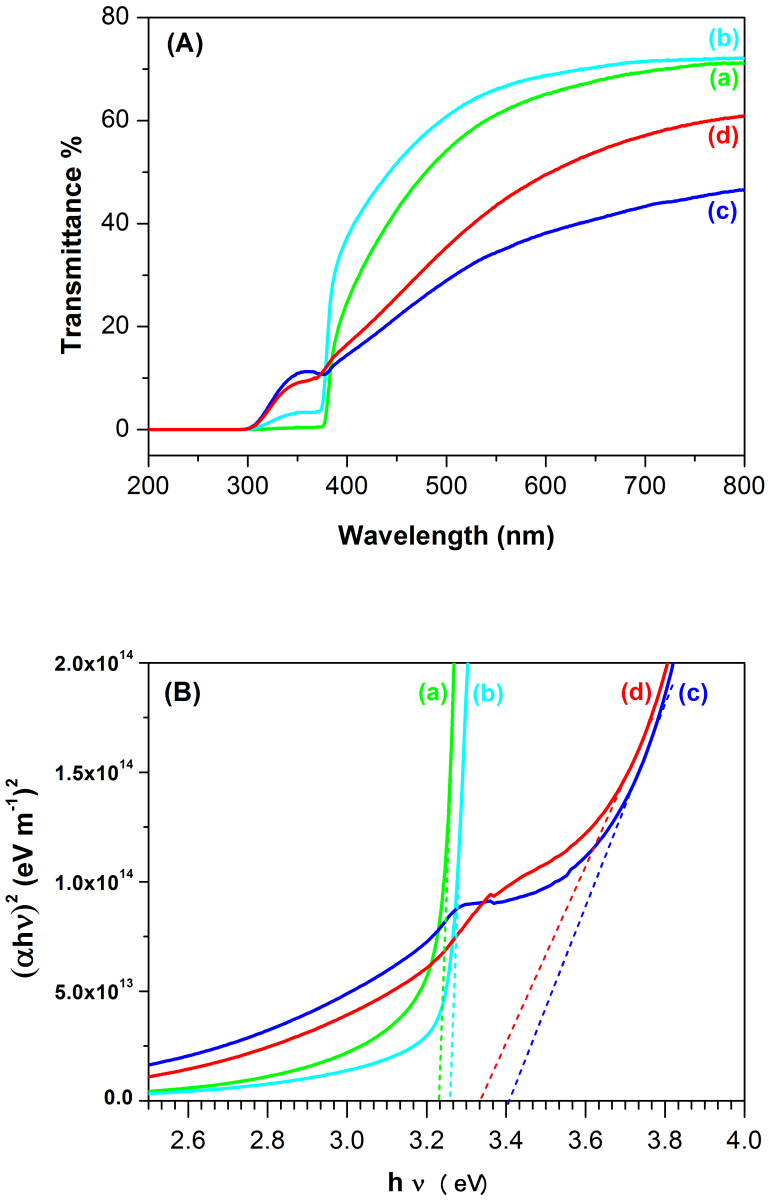

Figure 4: (Color online) (A) Transmittance (T) and (B) $(\alpha h\nu)^2$ vs. phonon energy $h\nu$. (a) 0.0, (b) 1.5, (c) 4.0 and (d) 5.5 at.%Sm.

3.3.2. Photoluminescence

Photoluminescence (PL) spectra of pure and Sm doped ZnO nanorods measured at room temperature with excitation wavelength 341 nm is shown in Fig. 5. PL is also known as one of the most effective techniques to detect the present of defects in semiconductors. Two emissions are observed in PL spectra, UV and visible light emission. Our PL results are in good agreement with the previously reported Sm doped ZnO thin film prepared by sputtering assisted metalorganic chemical vapour deposition [21]. The UV emission, ~ 401 nm is also known as near band edge emission of ZnO and it is due to the free-exciton recombination process through exciton-exciton collisions [48, 49]. It should be noted that the UV emission shows a small peak around 388 nm and it becomes more pronounce with increasing the Sm content (see Fig. 5). This peak may be attributed to the transition in energy in ZnO between an

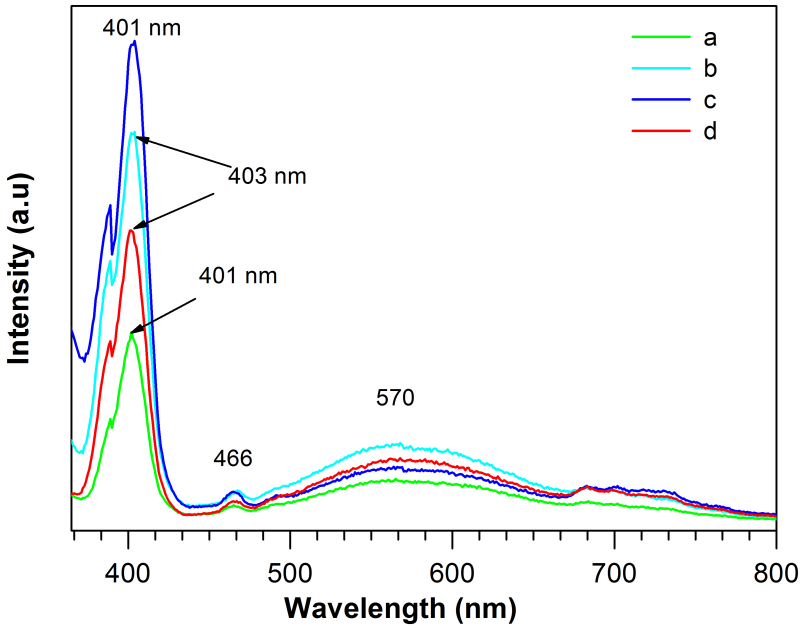

Figure 5: (Color online) Room temperature PL for: (a) 0 at.%Sm, (b) 1.5 at.%Sm, (c) 4 at.%Sm and (d) is 5.5 at.%Sm in ZnO.

electron in Zn interstitial defect states and a hole in the valence band. The presence of strong UV emission of pure and Sm doped ZnO nanorods in PL spectra indicate that the as-synthesized samples have a good crystal quality with excellent optical properties compared to work reported by Jingyuan *et al.* [18] and Velusamy and co-workers [50]. PL results are in good agreement with XRD and Raman scattering spectroscopy results discussed in preceding sections above. From Fig. 5 it can be observed that at the Sm content (4.0 and 5.5 at.% Sm) the UV peak was red shifted slightly to 403 nm. The as-synthesized samples shows blue emission at 466 nm which is has been reported as the Zn interstitial or quantum confinement [51]. The broad emission (deep-level emission) in the green-yellow part of the visible light spectrum is due to different point defects, either intrinsic [52, 53, 54] or extrinsic [55]. Vanheusden *et al.* [56] reported that single oxygen vacancies in the ZnO nanomaterials are responsible for the green-yellow emission. The donor-acceptor transition has been also proposed as origin of the green-yellow emission [57]. Furthermore, zinc vacancy and surface defect have also been proposed as the cause of the green emission [51, 58]. The origin of the green emission is debatable and needs further study to determine the origin of the green emission. In our case doping ZnO nanorods with Sm introduces more oxygen vacancies, which could be responsible for the green-yellow emission. The presence of oxygen vacancies are confirmed with results from XPS as will be discussed in the following section. Nevertheless, Sm doped ZnO nanorods enhanced the green-yellow emission in the visible light part compared to the pure ZnO nanorods. Our results are similar to the previously reported on ZnO nanorods doped with Sm on Si substrate [59]. It is, however, also shown in Fig. 5 that the green-yellow emission intensity decreased at higher concentration (5.5 at.% Sm). Similar phenomena have been observed when ZnO nanorods were doped with Ce and N [60, 61]. The decrease in the intensity at higher concentration of dopant is due to the crystal defects, which increased scattering of phonons. The defects seen by PL are in good agreements with results from Raman scattering (see Fig. 3).

3.3.3. X-ray photoelectron spectroscopy

Fig. 6 shows the survey XPS spectra measured for Sm-doped ZnO nanorods on ITO. Fig. 7 (a) shows a comparison of the Zn 2p core level spectra. The line shape reveals single $2p_{3/2}$ and $2p_{1/2}$ peaks, which are located at 1021.1 eV and 1044.2 eV binding energies, respectively. This reveals that Zn atoms are in a 2+ oxidation state, consistent with previous XPS studies on ZnO nanorods [35, 62]. This is attributed to the Zn atoms in the ZnO bulk crystal structure. Line shape and binding energies do not change with doping. This shows that the Zn electronic structure is not affected by Sm doping.

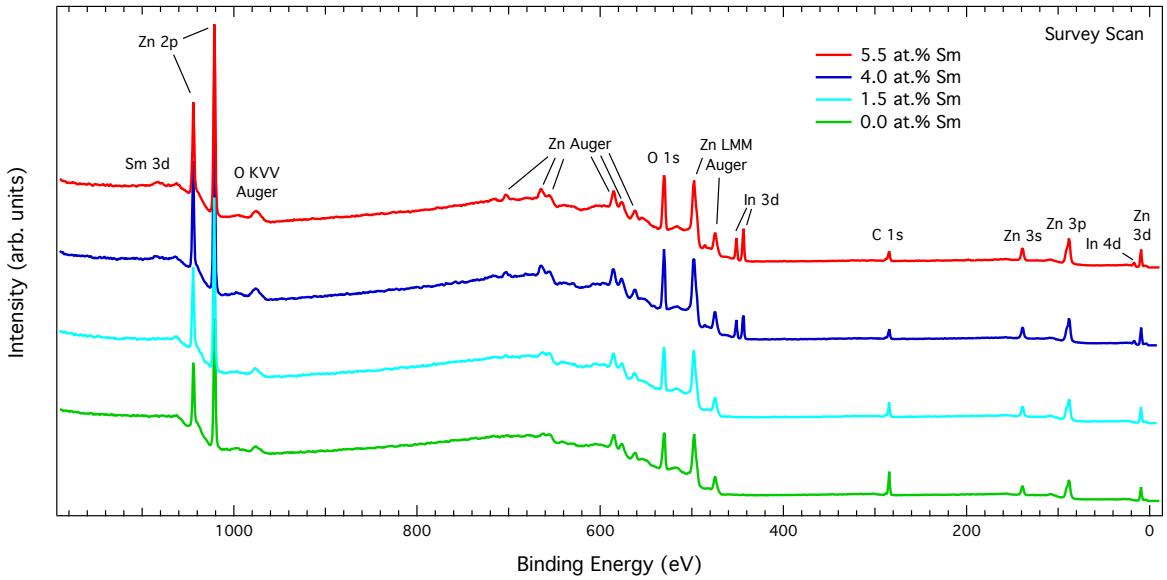

Figure 6: (Color online) Survey XPS spectra for Sm-doped ZnO nanorods on ITO in the binding energy range from 1190 eV to -10 eV. Core level and Auger peaks have been named accordingly.

Fig. 7 (b) shows that the Zn 3p core level line shape is also unaffected by the doping. It comprises of two peaks, $3p_{3/2}$ and $3p_{1/2}$, located at 88.03 eV and 90.03 eV, separated by a spin-orbit splitting of 2.0 eV, as expected for Zn. Fig. 8 shows a comparison of the O 1s XPS core level spectra. The O 1s peak is composed of two subcomponents: the main peak (labelled peak 1) on the lower binding energy side is attributed to the stoichiometric oxygen ions in the main ZnO matrix, while its higher binding energy shoulder (peak 2) is attributed to oxygen vacancies. Therefore, the XPS indicate the presence of oxygen vacancies increased within the Sm doped ZnO nanorods. The fitting parameters are reported in Table 3. Which is in accordance to the PL results as described in the preceding section.

Table 3: Fit parameters for O 1s core level as a function of Sm doping.

at.%Sm	BE(1) (eV)	BE(2) (eV)	area ratio (1/2)
0.0	529.80	531.39	1.66
1.5	529.88	531.38	1.10
4.0	529.93	531.48	1.42
5.5	529.76	531.41	1.39

3.4. Electrical characterization

Fig. 9 shows semilogarithmic *I-V* characteristics of Pd/ZnO/ITO Schottky diodes fabricated on undoped and Sm doped ZnO nanorods, measured at room temperature. The nanorods underneath the Pd contacts could be taken as a collection of single Schottky diodes aligned in parallel. As can be seen from Fig. 9 (A) and (B) the rectification behavior is positively improved when doping with Sm (1.5 at.%) at applied voltage ±1 V. The difference between forward and revers current at 1.5 at.% is almost two and half orders of magnitude compared to undoped samples. Our results for undoped samples are similar to previously reported on ZnO Schottky diodes prepared using the CBD technique [63]. However, for Sm doped ZnO nanorods at 4.0 and 5.5 at.% (not shown) there was no rectification. This could be due to the Sm doping or poor contact between the Pd and the nanorods. The current-voltage characteristic in the forward bias of the Schottky diodes can be well described using thermionic emission theory and its given by [64]:

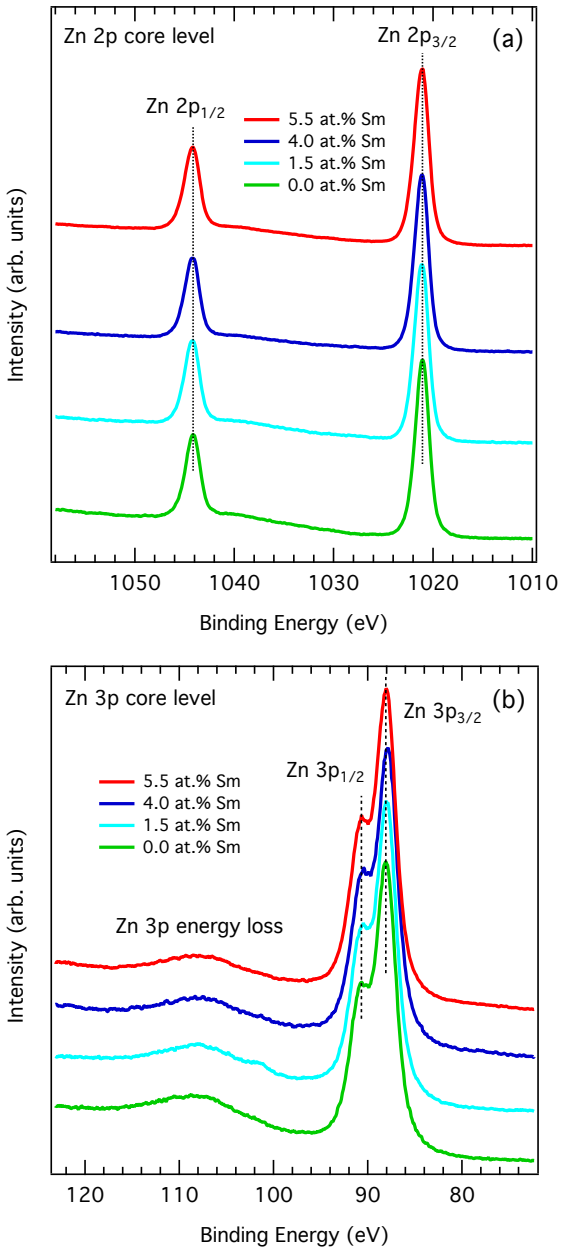

Figure 7: (Color online) Zn 2p (a) and Zn 3p (b) core level XPS spectra for Sm-doped ZnO nanorods on ITO.

$$I = I_0 \left[1 - exp\left(\frac{-q(V - IRs)}{K_B T} \right) \right] \tag{6}$$

where, q is the electronic charge, R_s is the series resistance and I_0 is the saturation current in the absence of external bias and it is given by:

$$I_0 = S A^* T^2 [-q \frac{\Phi_{B_0}}{n K_B T}] \tag{7}$$

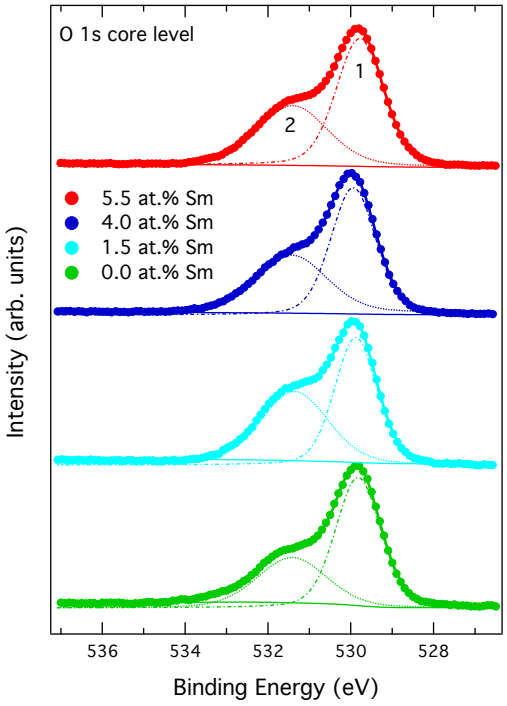

Figure 8: (Color online) O 1s core level XPS spectra for Sm-doped ZnO nanorods on ITO. Spectra have been normalized to the area of peak 1 for better comparison. Refer to the main text for further explanations.

where, A^* is the effective Richardson constant, K_B is the Boltzmann constant, T is the absolute temperature, S is the diode contact area, Φ_{B_0} is the Schottky barrier height and n is the diode ideality factor. The n values obtained from the fit were 4.8 and 2.5 for undoped and Sm doped ZnO nanorods at 1.5 %, respectively. These values are higher compared to ideal diode ($n = 1$) which could be attributed to some reasons such as series resistance, voltage drop across the metal semiconductor junction, surface and interface states [65]. Furthermore, Schottky diodes fabricated using chemical solutions in air can induce interfacial dielectric layers that affect the current transport across the diode [66]. The obtained Φ_{B_0} values from the fit for undoped and Sm doped ZnO nanorods at 1.5 at.% were found to be 0.55 eV and 0.72 eV, respectively. The deviation of these values from the theoretically calculated one (difference between Pd work function and ZnO electron affinity) could be due to some factors. For examples, non-homogeneous barrier formation, poor contact between Pd/ZnO [63], deviation from the linearity of I-V characteristic and Sm doping could probably cause this deviation.

4. Conclusion

Pure and Sm doped ZnO nanorods were successfully synthesized on seeded ITO glass substrates using the chemical bath deposition method. XRD results revealed that Sm^{+3} has been successfully incorporated into the ZnO lattice structure and no other impurities or other phases from Sm were detected. The growth rate of the nanorods was suppressed by the Sm doping ZnO nanorods as seen by FE-SEM where the density and length of the nanorods decreased upon Sm doping concentration. Raman spectra revealed high crystalline hexagonal wurtzite ZnO structure by having sharp and intense E_2 (high) mode. However, the FWHM increased with increasing Sm doping concentrations indicating that more defects were introduced into the ZnO nanorods. The UV-vis transmittance revealed that the Sm doping ZnO nanorods has widened the optical band gap. The PL spectra shows both strong UV emission located at 400 nm along with small peak positioned at 388 nm and broad peak (green-yellow band) in the visible region. All the samples displayed strong UV emission peak indicating high crystal quality of the as-synthesized samples. The deep-level

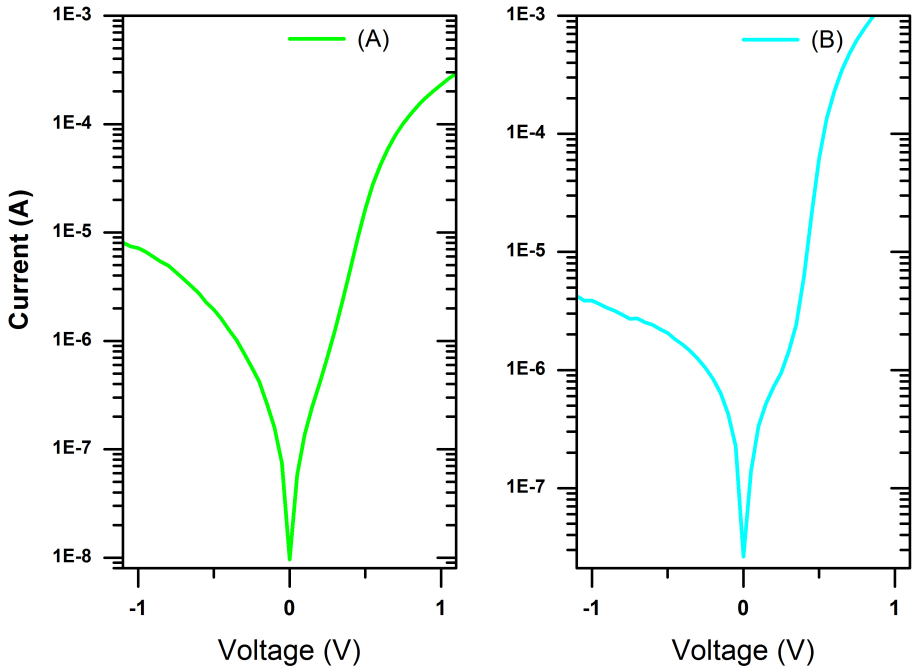

Figure 9: (Color online) semilogarithmic *I-V* characteristic of (A) pure ZnO nanorods and (B) Sm doped ZnO nanorods at 1.5 at.%.

emission peak intensities were enhanced with increasing Sm content indicating more defects were introduced which agreed well with Raman scattering results. The XPS results revealed the presence of Zn and O with small amount of C used for calibration and Sm in the 5.5 at.% Sm doped ZnO. Moreover, the XPS analysis showed the presence of oxygen vacancies within the Sm doped and undoped ZnO nanorods. The *I-V* curve showed that the rectifying behavior of Schottky diodes is improved when ZnO nanorods are doped with Sm at 1.5 at.%. The contrast between forward and revers current were two and half orders of magnitude for Sm doped ZnO at 1.5 at.% compared to undoped ZnO.

Acknowledgment

This work is supported by the South African Research Foundation (NRF) grant No. 93205. The author would like to thank Dr. Shankara, from department of Chemistry at the University of Pretoria for the UV-vis measurements and the author also wish to thanks Prof. Hendrik Swart at the University of Free State for PL measurements.

References

[1] A. Kathalingam, D. Vikraman, H. S. Kim, H. J. Park, Facile fabrication of n-ZnO nanorods/p-Cu_2O heterojunction and its photodiode property, Opt. Mater. 66 (2017) 122–130.
[2] Y. R. Ryu, T. S. Lee, J. A. Lubguban, H. W. White, Y. S. Park, C. J. Youn, ZnO devices: Photodiodes and p-type field-effect transistors, Appl. Phys Lett. 87 (15) (2005) 153504.
[3] L. Luo, Y. Zhang, S. S. Mao, L. Lin, Fabrication and characterization of ZnO nanowires based UV photodiodes, Sens. Actuators A: Phys. 127 (2) (2006) 201 – 206.
[4] J. Huang, L. Wang, R. Xu, K. Tang, W. Shi, Y. Xia, Growth of p-type ZnO films and fabrication of ZnO photodiode-based UV detectors, Semicond. Sci. Technol. 24 (7) (2009) 075025.
[5] Z. Fan, D. Wang, P. C. Chang, W. Y. Tseng, J. G. Lu, ZnO nanowire field-effect transistor and oxygen sensing property, Appl. Phys. Lett. 85 (24) (2004) 5923–5925.
[6] X. Wang, J. Zhou, J. Song, J. Liu, N. Xu, Z. L. Wang, Piezoelectric field effect transistor and nanoforce sensor based on a single ZnO nanowire, Nano. lett. 6 (12) (2006) 2768–2772.

[7] S. Baek, J. Song, S. Lim, Improvement of the optical properties of ZnO nanorods by Fe doping, Physica B: Condens. Matt. 399 (2) (2007) 101–104.
[8] G. Murugadoss, Synthesis and characterization of transition metals doped ZnO nanorods, J. Mater. Sci. Technol. 28 (7) (2012) 587–593.
[9] A. Ishizumi, Y. Taguchi, A. Yamamoto, Y. Kanemitsu, Luminescence properties of ZnO and Eu^{+3} doped ZnO nanorods, Thin Solid Films 486 (1) (2005) 50–52.
[10] K. T. Ramakrishna Reddy, R. W. Miles, Growth and characterization of sprayed ZnO :Ga thin films, J. Mater. Sci. Lett. 17 (4) (1998) 279–281.
[11] S. Kurtaran, S. Aldag, G. Ofofoglu, I. Akyuz, F. Atay, On the role of Al in ultrasonically sprayed ZnO films, Mater. Chem. Phys. 185 (2017) 137–142.
[12] T. Terasako, H. Song, H. Makino, S. Shirakata, T. Yamamoto, Temperature dependence of electrical properties of Ga-doped ZnO films deposited by ion plating with DC arc discharge, Thin Solid Films 528 (2013) 19–25.
[13] K. Nagaraja, S. Pramodini, A. S. Kumar, H. Nagaraja, P. Poornesh, D. Kekuda, Third-order nonlinear optical properties of Mn doped ZnO thin films under cw laser illumination, Opt. Mater. 35 (3) (2013) 431–439.
[14] A. Antony, S. Pramodini, P. Poornesh, I. Kityk, A. Fedorchuk, G. Sanjeev, Influence of electron beam irradiation on nonlinear optical properties of Al doped ZnO thin films for optoelectronic device applications in the cw laser regime, Opt. Mater. 62 (2016) 64–71.
[15] P. Korake, A. Kadam, K. Garadkar, Photocatalytic activity of Eu^{3+}-doped ZnO nanorods synthesized via microwave assisted technique, J. Rare Earths 32 (4) (2014) 306–313.
[16] A. Urbieta, R. del Campo, R. Pérez, P. Fernández, J. Piqueras, Luminescence and waveguiding behavior in Tb doped ZnO micro and nanostructures, J. Alloy Compd. 610 (2014) 416–421.
[17] R. Zamiri, A. Lemos, A. Reblo, H. A. Ahangar, J. Ferreira, Effects of rare-earth (Er, La and Yb) doping on morphology and structure properties of ZnO nanostructures prepared by wet chemical method, Ceram. Int. 40 (1) (2014) 523–529.
[18] J. Piao, L. Tseng, J. Yi, Ferromagnetism in Sm doped ZnO nanorods by a hydrothermal method, Chem. Phys. Lett. 649 (2016) 19–22.
[19] V. Kumar, S. Som, V. Kumar, V. Kumar, O. Ntwaeaborwa, E. Coetsee, H. Swart, Tunable and white emission from ZnO: Tb^{3+} nanophosphors for solid state lighting applications, Chemical Engineering Journal 255 (2014) 541–552.
[20] X. Zeng, J. Yuan, Z. Wang, L. Zhang, Nanosheet-based microspheres of Eu^{3+}-doped ZnO with efficient energy transfer from ZnO to Eu^{3+} at room temperature, Adv. Mater. 19 (24) (2007) 4510–4514.
[21] T. Tsuji, Y. Terai, M. Hakim, M. Kawabata, Y. Fujiwara, Photoluminescence properties of Sm-doped ZnO grown by sputtering-assisted metalorganic chemical vapor deposition, J. Non Cryst. Solids 358 (17) (2012) 2443–2445.
[22] H. He, J. Fei, J. Lu, Sm-doping effect on optical and electrical properties of ZnO films, J. Nanostruct. Chem. 5 (2) (2015) 169–175.
[23] Z. B. Ayadi, L. El Mir, K. Djessas, S. Alaya, Electrical and optical properties of aluminum-doped zinc oxide sputtered from an aerogel nanopowder target, Nanotechnology 18 (44) (2007) 445702.
[24] K. Tang, S. Gu, S. Li, J. Ye, S. Zhu, H. Chen, J. Liu, R. Zhang, Y. Shi, Y. Zheng, Influence of thermally diffused aluminum atoms from sapphire substrate on the properties of ZnO epilayers grown by metal-organic chemical vapor deposition, J. Vac. Sci. Technol. A: Vac. Surf. Films 29 (3) (2011) 03A106.
[25] O. Novodvorsky, L. Gorbatenko, V. Y. Panchenko, O. Khramova, Y. A. Cherebilo, C. Wenzel, J. Bartha, V. Bublik, K. Shcherbachev, Optical and structural characteristics of Ga-doped ZnO films, Semiconductors 43 (4) (2009) 419–424.
[26] A. S. Hussein, Z. Hassan, S. Thahab, S. Ng, H. A. Hassan, C. Chin, Effect of Al mole fraction on structural and electrical properties of Al_x Ga_{1-x} N/GaN heterostructures grown by plasma-assisted molecular beam epitaxy, Appl. Surf. Sci. 257 (9) (2011) 4159–4164.
[27] G. Murugadoss, Structural and optical properties of monodispersed ZnS/CdS/ZnO and ZnO /ZnS/CdS nanoparticles, J. Lumin. 132 (10) (2012) 2665–2669.
[28] L. Vayssieres, K. Keis, S. Lindquist, A. Hagfeldt, Purpose-built anisotropic metal oxide material: 3D highly oriented microrod array of ZnO, J. Phys. Chem. B 105 (17) (2001) 3350–3352.
[29] L. Vayssieres, Growth of arrayed nanorods and nanowires of ZnO from aqueous solutions, Adv. Mater. 15 (5) (2003) 464–466.
[30] B. Cao, W. Cai, Y. Li, F. Sun, L. Zhang, Ultraviolet-light-emitting ZnO nanosheets prepared by a chemical bath deposition method, Nanotechnology 16 (9) (2005) 1734 – 1738.
[31] W. Chebil, A. Fouzri, A. Fargi, B. Azeza, Z. Zaaboub, V. Sallet, Characterization of ZnO thin films grown on different p-Si substrate elaborated by solgel spin-coating method, Mater. Res. Bull. 70 (2015) 719–727.
[32] N. A. Jayah, H. Yahaya, M. R. Mahmood, T. Terasako, K. Yasui, A. Hashim, High electron mobility and low carrier concentration of hydrothermally grown ZnO thin films on seeded a-plane sapphire at low temperature, Nanoscale Res. lett. 10 (1) (2015) 7.
[33] W. Park, G. Yi, Electroluminescence in n-ZnO Nanorod Arrays Vertically Grown on p-GaN, Adv. Mater. 16 (1) (2004) 87–90.
[34] P. Dhamodharan, C. Manoharan, M. Bououdina, R. Venkadachalapathy, S. Ramalingam, Al-doped ZnO thin films grown onto ITO substrates as photoanode in dye sensitized solar cell, Solar Energy 141 (2017) 127–144.
[35] J. Zheng, Q. Jiang, J. Lian, Synthesis and optical properties of flower-like ZnO nanorods by thermal evaporation method, Appl. Surf. Sci. 257 (11) (2011) 5083–5087.
[36] G. Murtaza, M. Iqbal, Y. Xu, I. Will, Z. Huang, Study of Sm-doped ZnO samples sintered in a nitrogen atmosphere and deposited on n-Si (100) by evaporation technique, J. Magn.and Magn. Mater. 323 (24) (2011) 3239–3245.
[37] D. Arora, K. Asokan, A. Mahajan, H. Kaur, D. Singh, Structural, optical and magnetic properties of Sm doped ZnO at dilute concentrations, RSC Advances 6 (81) (2016) 78122–78131.
[38] Z. Sofiani, B. Derkowska, P. Dalasiński, M. Wojdyła, S. Dabos-Seignon, M. A. Lamrani, L. Dghoughi, W. Bała, ó. Addou, B. Sahraoui, Optical properties of ZnO and ZnO : Ce layers grown by spray pyrolysis, Opt. Commun. 267 (2) (2006) 433–439.
[39] J. Wang, C. Ponton, I. Harris, A study of Pr-substituted strontium hexaferrite by hydrothermal synthesis, J. Alloys Compd. 403 (1) (2005) 104–109.
[40] U. Holzwarth, N. Gibson, The scherrer equation versus the'Debye-Scherrer equation', Nat. Nanotechnol. 6 (9) (2011) 534–534.
[41] R. Cuscó, E. Alarcón-Lladó, J. Ibáñez, L. Artús, J. Jiménez, B. Wang, M. J. Callahan, Temperature dependence of Raman scattering in ZnO, Phys. Rev. B 75 (16) (2007) 165202.
[42] C. A. Arguello, D. L. Rousseau, S. P. S. Porto, First-order Raman effect in wurtzite-type crystals, Phys. Rev. 181 (3) (1969) 1351 – 1363.

[43] C. Du, Z. Gu, M. Lu, J. Wang, S. Zhang, J. Zhao, G. Cheng, H. Heng, Y. Chen, Raman spectroscopy of (Mn, Co)-codoped ZnO films, J. Appl. Phys. 99 (12) (2006) 123515.
[44] J. Zeng, J. K. Low, Z. M. Ren, T. Liew, Y. F. Lu, Effect of deposition conditions on optical and electrical properties of ZnO films prepared by pulsed laser deposition, Appl. Surf. Sci. 197 (2002) 362–367.
[45] J. Chen, D. Chen, J. He, S. Zhang, Z. Chen, The microstructure, optical, and electrical properties of sol-gel-derived Sc-doped and Al-Sc co-doped ZnO thin films, Appl. Surf. Sci. 255 (23) (2009) 9413–9419.
[46] C. Wu, J. Shen, J. Ma, S. Wang, Z. Zhang, X. Yang, Electrical and optical properties of molybdenum-doped ZnO transparent conductive thin films prepared by dc reactive magnetron sputtering, Semicond. Sci. Techol. 24 (12) (2009) 125012.
[47] V. Kumari, V. Kumar, B. Malik, R. Mehra, D. Mohan, Nonlinear optical properties of erbium doped zinc oxide (ezo) thin films, Opt. Commun. 285 (8) (2012) 2182–2188.
[48] M. H. Huang, Y. Wu, H. Feick, N. Tran, E. Weber, P. Yang, Catalytic growth of zinc oxide nanowires by vapor transport, Adv. Mater. 13 (2) (2001) 113–116.
[49] Y. C. Kong, D. P. Yu, B. Zhang, W. Fang, S. Q. Feng, Ultraviolet-emitting ZnO nanowires synthesized by a physical vapor deposition approach, Appl. Phys. Lett. 78 (4) (2001) 407–409.
[50] P. Velusamy, R. R. Babu, K. Aparna, Effect of Sm doping on the physical properties of ZnO thin films deposited by spray pyrolysis technique, in: AIP Conf. Proceedings, Vol. 1832, AIP Publishing, 2017, p. 080085.
[51] A. Djurišić, W. Choy, V. Roy, Y. Leung, C. Kwong, K. Cheah, T. Gundu Rao, W. Chan, H. Fei Lui, C. Surya, Photoluminescence and electron paramagnetic resonance of ZnO tetrapod structures, Adv. Funct. Mater. 14 (9) (2004) 856–864.
[52] R. Zhang, P. Yin, N. Wang, L. Guo, Photoluminescence and Raman scattering of ZnO nanorods, Solid State Sci. 11 (4) (2009) 865–869.
[53] V. A. Fonoberov, A. A. Balandin, Origin of ultraviolet photoluminescence in ZnO quantum dots: Confined excitons versus surface-bound impurity exciton complexes, Appl. Phys. lett. 85 (24) (2004) 5971–5973.
[54] B. K. Meyer, H. Alves, D. M. Hofmann, W. Kriegseis, D. Forster, F. Bertram, J. Christen, A. Hoffmann, M. Straßburg, M. Dworzak, et al., Bound exciton and donor–acceptor pair recombinations in ZnO, Phys. Status Solid. B 241 (2) (2004) 231–260.
[55] R. Dingle, Luminescent transitions associated with divalent copper impurities and the green emission from semiconducting zinc oxide, Phys. Rev. Lett. 23 (11) (1969) 579–581.
[56] K. Vanheusden, W. Warren, C. Seager, D. Tallant, J. Voigt, B. Gnade, Mechanisms behind green photoluminescence in ZnO phosphor powders, J. of Appl. Phys. 79 (10) (1996) 7983–7990.
[57] Y. Wang, S. Lau, X. Zhang, H. Lee, S. Yu, B. Tay, H. Hng, Evolution of visible luminescence in ZnO by thermal oxidation of zinc films, Chem. Phys. Lett. 375 (1) (2003) 113–118.
[58] Y. Heo, D. Norton, S. Pearton, Origin of green luminescence in ZnO thin film grown by molecular-beam epitaxy, J. Appl. Phys. 98 (7) (2005) 073502.
[59] C. Lin, S. Young, C. Kung, L. Horng, H. Chen, M. Kao, Y. Shih, C. Ou, Phonon spectra and magnetic behaviors of hydrothermally synthesized Sm-doped ZnO nanorods, Vacuum 87 (2013) 178–181.
[60] C. Chang, C. Lin, J. Chen, M. Hsu, Ce-doped ZnO nanorods based low operation temperature NO_2 gas sensors, Ceram. Int. 40 (7) (2014) 10867–10875.
[61] K. Mahmood, S. B. Park, Growth and conductivity enhancement of N-doped ZnO nanorod arrays, J. Cryst. Growth 347 (1) (2012) 104–112.
[62] X. C. L. Y. Xu, C., C. Wang, A simple and novel route for the preparation of ZnO nanorods, Solid State Commun. 122 (3-4) (2002) 175–179.
[63] B. S. Mwankemwa, M. J. Legodi, M. Mlambo, J. M. Nel, M. Diale, Structural, morphological, optical and electrical properties of schottky diodes based on CBD deposited ZnO: Cu nanorods, Superlattices Microstruct. 107 (2017) 163–171.
[64] E. Rhoderick, R. Williams, M.-S. Contacts, 2nd edn, Clarendon, Oxford.
[65] N. S. Singh, L. Kumar, A. Kumar, S. Vaisakh, S. D. Singh, K. Sisodiya, S. Srivastava, M. Kansal, S. Rawat, T. A. Singh, et al., Fabrication of zinc oxide/polyaniline (ZnO/PANI) heterojunction and its characterisation at room temperature, Mater. Sci. Semicond. Process. 60 (2017) 29–33.
[66] L. J. Brillson, Y. Lu, ZnO Schottky barriers and ohmic contacts, J. Appl. Phys. 109 (12) (2011) 8.